crystals

MDPI

Article

A Tunable NIR Filter with Sphere Phase Liquid Crystal

Changli Sun and Jiangang Lu *

Department of Electronic Engineering, Shanghai Jiao Tong University, Shanghai 200240, China
* Correspondence: lujg@sjtu.edu.cn; Tel.: +86-21-3420-7914

Received: 7 June 2019; Accepted: 6 July 2019; Published: 8 July 2019

Abstract: A near-infrared (NIR) filter with sphere phase liquid crystal (SPLC) is proposed, which shows a low operating electric field and large temperature-gradient modulations. The central wavelength of the Bragg reflection can be thermally tuned from 1580 nm to 1324 nm with a temperature-gradient of 42.7 nm/K. Meanwhile, the central wavelength can be electrically tuned over 76 nm within a low operating electric field of 0.3 V/μm. Thus, the SPLC filter may achieve a wavelength variation of 256 nm by thermal modulation and 76 nm by electrical modulation. The SPLC filter shows great potential applications in optical communication devices.

Keywords: liquid-crystal devices; filter; liquid crystals

1. Introduction

Optical filters have been widely used in various optical devices and systems, especially in the optical communication field [1,2]. Various types of optical filters have been developed such as the Mach-Zehnder interferometer (MZI) filter [3], Fabry-Perot cavities [4], Fibonacci quasi-periodic grating [5], and Bragg grating filter [6]. However, the tuning range dramatically limits their application. Liquid crystal (LC) materials with periodic structures exhibit a high potential for considerable use in broadening the tuning range such as cholesteric liquid crystal (CLC) [7,8], chiral smectic liquid crystal [9], and blue phase (BP) [10,11]. These materials are also used in filters due to their flexible tunability in external perturbations such as temperature, electric field, light, spatial variation, and so on. Yuhua Hang et al. investigated the optical filter with the central wavelength tuned from 826 nm to 517 nm by changing the temperature on two CLC samples with a temperature-gradient of 19.1 nm/K [12]. Sung-Taek Hur et al. prepared a dye-doped liquid crystalline cubic BP cell with a wide tuning range of about 150 nm and a temperature-gradient of 6 nm/K [13]. A filter with the central wavelength tuned from 573 nm to 500 nm with a temperature-gradient of 2.6 nm/K by using both right- and left-handed CLCs has also been proposed [8]. Jiade Lin et al. reported a continuously tunable photonic bandgap with a wide spectral range of about 130 nm using the spatial tuning method based on a blue phase wedge cell [11]. A shift of the reflection band from 1217 nm to 1575 nm was observed in CLCs when the voltage was applied from 170 V to 215 V with an electric field of 4.89 V/μm [7]. Eva Oton et al. realized a dual frequency cholesteric liquid crystal device with the color shift from 530 nm to 635 nm by applying an electrical field of over 20 V/μm at different frequencies [14]. In spite of the remarkable achievements in realizing the filtering performance using novel materials and methods, the tunable speed, fabricated process, and driving capacity still need to be improved for further applications.

In this work, we demonstrate a tunable NIR filter based on sphere phase liquid crystal (SPLC). The sphere phase, usually observed between the isotropic phase (Iso) and chiral nematic phase (N*) or between the isotropic phase and blue phase, has been demonstrated by Jiliang Zhu [15–18]. Like the BPLC, the SPLC is composed of self-assembly periodic helical structures and disclinations among

them, as shown in Figure 7 [15]. As the periodic helical structure, the three-dimensional twist sphere (3-DTS) structure looks like a sphere structure, so is termed as the sphere phase. On the outermost circumference of the double twist structure, the molecules are twisted by 45° in respect of the z-axis with +45° at one end and −45° at the other end. Unlike the macro optical isotropic status in BPLC, the SPLC shows an optical anisotropic status. The Bragg reflection of blue phase liquid crystal originates from the periodic double-twisted cylinder (DTC) lattice structure of nano-scale pitch, leading to the Bragg wavelength in the visible band. Whilst in the sphere phase, the 3-DTS structure consists of several planar layers of double twist molecules, and the twisted angle of molecules on the outermost circumferences decreases from the equatorial plane to the poles in 3-DTS. The CLC also consists of several planar layers, which is similar to that of SPLC, and the pitch of CLC can reach up to 2.5 μm [7]. Therefore, the central wavelength of SPLC is enabled to extend to the NIR band due to the 3-DTS structure, and will red-shift with decreasing concentration of the chiral dopant in the mixture. Meanwhile, due to the small anchoring energy, SPLC shows sensitivity to external perturbations such as temperature and electric field, providing potential applications for optical filters. In this paper, we demonstrate the transmission properties of SPLC in external perturbations including temperature and electric field. As there are diverse possibilities in the arrangement of three-dimensional twist spheres, the accurate equivalent phase distribution could not be confirmed. Therefore, the theoretical transmittance spectra of SPLC are not shown in this paper. The transmission properties of SPLC were analyzed with the experimental results. The Bragg reflection central wavelength can be thermally tuned with a large temperature-gradient and electrically tuned within a low operating electric field. The SPLC filter may achieve a wavelength variation of 256 nm by thermal modulation and 76 nm by electrical modulation.

2. Materials and Device Fabrication

To induce the 3-DTS structures, 1 wt. % chiral dopant (R5011, HCCH) was mixed with 99 wt. % nematic LC host, HC-1015X (Δn = 0.15, $\Delta\varepsilon$ = 33 at λ = 589 nm, and T = 293 K, HCCH). The precursor mixture was put (at 368 K) into an empty cell with a 20 μm cell gap, which comprised two indium-tin-oxide glass substrates with antiparallel polyimide alignment layers enhancing the reflection intensity. The mixture was cooled from the isotropic phase and sphere phase to the chiral nematic phase at a rate of 0.1 K/min using a temperature controller (HCS302, Instec Co., Boulder, Co, USA). The phase-transition behavior and platelet textures were observed under a polarized optical microscope (POM, XPL-30TF, Shanghai WeiTu Optics & Electron Technology Co., Ltd., Shanghai, China). A tungsten bromine lamp, as the unpolarized light source, provided the spectrum covering the NIR region. As the sphere phase was polarization dependent due to the spatial twist of liquid crystal molecules [15], a linear polarizer and quarter-wave plate were used to generate the right-circularly polarized light [19]. All the transmittance spectra were measured for the right-circularly polarized incident light [20,21]. All the Bragg reflection spectra from the sphere phase were collected by a detector attached to a data acquisition system (DCS300PA, Zolix, Beijing, China) as shown in Figure 1. Since the devices were fixed in the position, we characterized the properties of the NIR filter with transmittance spectra. The transmittance intensity of the transmittance spectra may be reduced by scattering from inhomogeneities, while the central wavelength, bandwidth, and the maximum transmissivity/reflectivity of the transmittance and reflectance spectra almost had the same values.

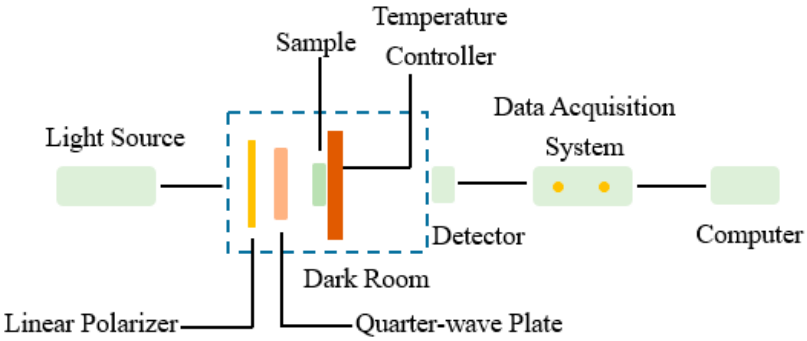

Figure 1. Schematic diagram of the transmittance measurement system.

During the cooling process at a rate of 0.1 K/min, the mixture showed the following phase sequence: Iso 351 K SP, 345 K SP & N*, 343 K N*, as shown in Figure 2. The pictures were observed in cells with antiparallel polyimide alignment layers by the POM. In order to avoid the Bragg reflection band, the characteristics of light scattering of the LC mixture at wavelengths out of the selective reflection band were illustrated, as shown in Figure 2e. When the temperature was above 351 K in the isotropic phase, the transmittance was insensitive to the temperature change because there was no periodic structure in the isotropic phase. The transmittance decreased from 351 K to 345 K in the sphere phase as the growth of the 3-DTS structures enhanced the scattering effect in the lattice formation process [15,18]. Additionally, the transmittance gradually increased at the SP-N* coexistence phase from 345 K to 343 K given the larger scattering effect of 3-DTS structures induced by the discontinuous grain boundaries between 3-DTSs than the one-dimensional periodic helical structure [17]. When the temperature was below 343 K in the chiral nematic phase, the transmittance was also insensitive to the temperature change because of the stable planar state of N* in the antiparallel cells. The experimental results indicate that the scattering caused by the 3-DTS structures of the sphere phase was stronger than that induced by the single-layer twist helical structures of the chiral nematic phase [17].

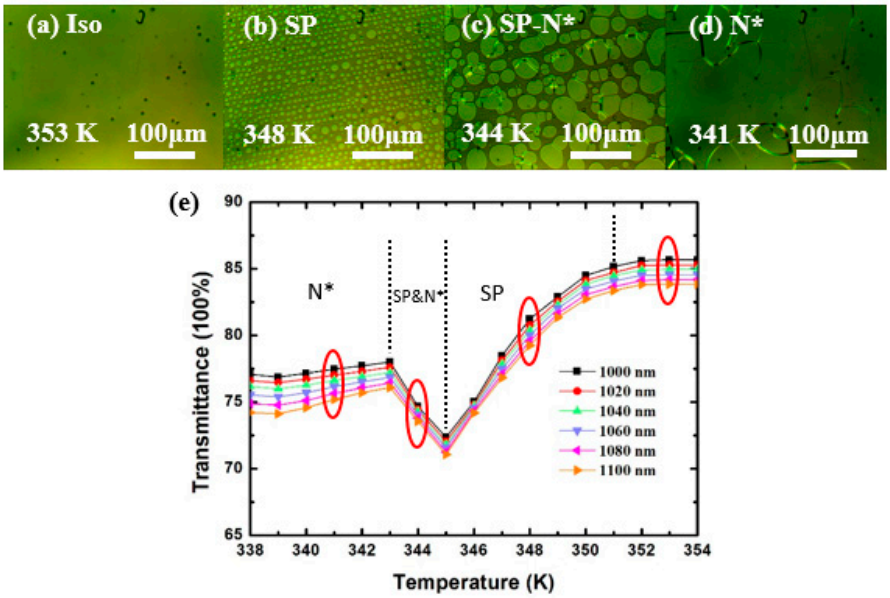

Figure 2. Polarizing microscope photographs of the mixture in phase transition from Iso to N*, (**a**) Iso, (**b**) SP, (**c**) SP-N*, and (**d**) N*, and (**e**) transmittance of the filter at SP, SP & N*, and N* versus temperature ranging from 338 K to 354 K.

3. Results and Discussion

The transmission spectra of the filter at SP, SP, and N*, and N* with temperature ranging from 338 K to 351 K are illustrated in Figure 3a, and the central wavelength variation with temperature change is shown in Figure 3b. If the temperature was higher than 351 K, no reflection band was observed as there is no helical structure at the isotropic phase. The central wavelength of the sphere phase shifted from 1580 nm to 1324 nm when the temperature decreased from 351 K to 345 K, corresponding to a temperature-gradient of 42.7 nm/K. During the cooling process from the sphere phase to N*, the structure changed from a multi-layer 3-DTS structure to a simple single-layer twist helical structure. At N* from 343 K to 338 K, the central wavelength only shifted from 1290 nm to 1234 nm with a temperature-gradient of 11.2 nm/K. The temperature-gradient marked with dashed lines in Figure 3b in the sphere phase was much larger than that at chiral nematic phase. The pitch in the sphere phase varied from 1034 nm to 864 nm with a temperature range from 351 K to 345 K, while the pitch at N* changed from 841 nm to 803 nm with a temperature range from 343 K to 338 K. The large temperature-gradient of sphere phase originated from the dramatic change of helical pitch, which was caused by the drastic tilt angle fluctuation of the LC molecules in the 3-DTS structures [15,22,23].

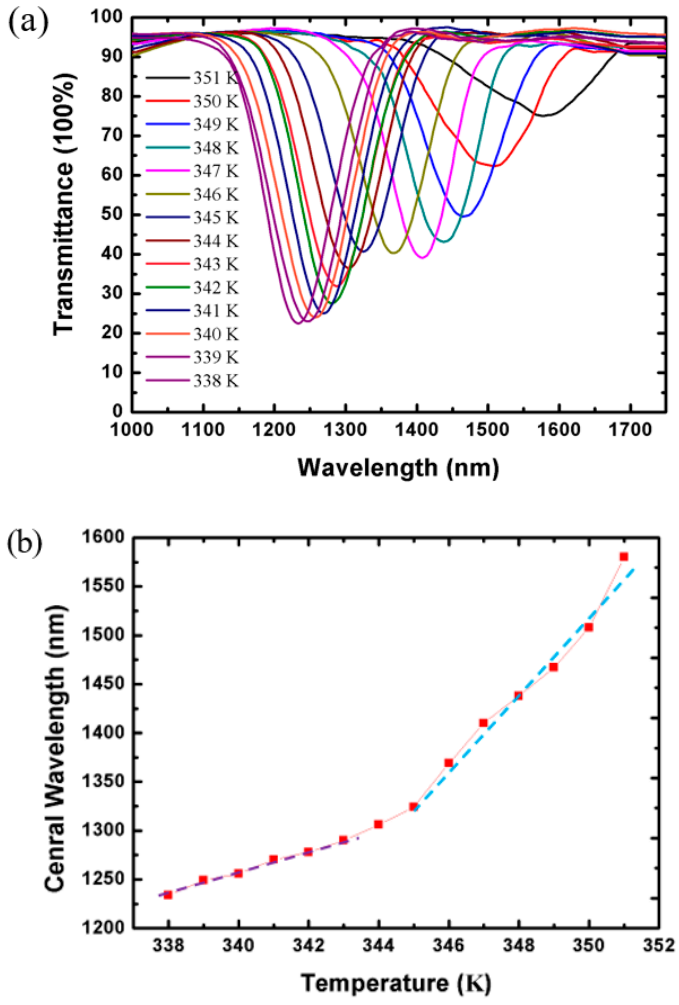

Figure 3. (**a**) Transmission spectra of the filter at SP, SP, and N*, and N* and (**b**) central wavelength variation with temperature change from 338 K to 351 K.

The temperature dependence of the central wavelength, λ, can be characterized by

$$\lambda(T) = n_{av}(T) \times P \quad (1)$$

where T is the temperature; P is the helical pitch; and $n_{av}(T)$ is the average refractive index of the mixture. The birefringence $\Delta n(T)$, the extraordinary refractive index $n_e(T)$, and the average refractive index $n_{av}(T)$ can be expressed as [24–26]:

$$\Delta n(T) = (\Delta n)_o(1 - \frac{T}{T_S})^{\beta} \tag{2}$$

$$n_e(T) = C - DT + \frac{2}{3}(\Delta n)_o(1 - \frac{T}{T_S})^{\beta} \tag{3}$$

$$n_{av}(T) = \sqrt{\frac{[C - DT + \frac{2}{3}(\Delta n)_o(1 - \frac{T}{T_S})^{\beta}]^2 + 2[C - DT - \frac{1}{3}(\Delta n)_o(1 - \frac{T}{T_S})^{\beta}]^2}{3}} \tag{4}$$

where the birefringence $(\Delta n)_o$ is defined as the difference between the extraordinary refractive index n_e and the ordinary refractive index n_o in the crystalline state, and T_S is the phase transition temperature between the isotropic phase and sphere phase. The material constants β, C, and D can be obtained by fitting the experimental results using Equations (2)–(4), and the measured refractive index data and fitting curves are shown in Figure 4. The dots represent the measured data and the lines are the fitting curves. The subscript "−e" and "−f" in the parameters represent the experimental data and the fitting data, respectively. As shown in Figure 4, the fitting values had a reasonable agreement with the experimental values.

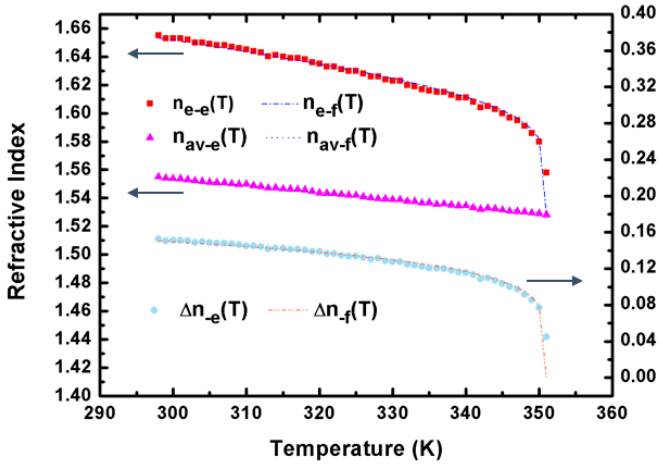

Figure 4. Measured refractive index versus the temperature and fitting curves.

The measured temperature dependence of pitch P in the system follows the empirical equation,

$$P = P_0 \cdot \left(1 - F \cdot \frac{T - T_C}{T_S - T_C}\right) \tag{5}$$

where F is the coefficient, and T_C is the critical temperature between the sphere phase and chiral nematic phase. The constant P_0 is the value of the pitch at Tc. The values of the coefficients for the sphere phase are listed as follows: $C = 1.69$, $D = 0.00046$, $(\Delta n)_o = 0.204$, $\beta = 0.161$, $F = -0.18$, $P_0 = 864$ nm, $T_C = 345$ K, and $T_S = 351$ K.

The electric field dependence of the central wavelength at different temperatures in the sphere phase was also investigated. A series of 1 kHz square-wave AC signals with different voltages were applied to the device. Figure 5 shows the textures of the sphere phase under a polarizing microscope at 345 K with different electric fields ranging from 0 V/μm to 0.3 V/μm. Upon increasing the electric field, the sphere texture shrank gradually due to the unwinding of the helical structure. Due to the small anchoring energy of the 3-DTS structures, when an external field of less than 0.3 V/μm is applied,

the texture tends to shrink and finally disappear, as shown in Figure 5d. The liquid crystal molecules in the 3-DTS structure reappeared when the electric field was removed due to the restoration of the 3-DTS structure.

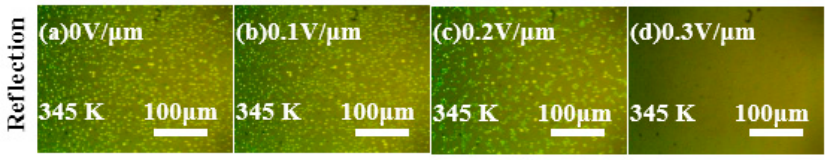

Figure 5. Polarizing microscope photographs of the mixture in the sphere phase with an electric field: (**a**) 0 V/μm, (**b**) 0.1 V/μm, (**c**) 0.2 V/μm, and (**d**) 0.3 V/μm.

The central wavelength of the transmittance spectra continuously varied within an electric field of 0.3 V/μm, giving a shift of 76 nm (from 1324 nm to 1248 nm) at 345 K (Figure 6a). Additionally, the transmissivity decreased gradually with the electric field because of the deformation of the 3-DTS structure. The average refractive index of LC mixture can be given by

$$n_{av} = \frac{n_{eff} + n_o}{2} = \frac{\frac{n_e n_o}{\sqrt{n_e^2 \cos^2\theta(E) + n_o^2 \sin^2\theta(E)}} + n_o}{2} \quad (6)$$

where n_{eff} is the effective refractive index, and the term $\theta(E)$ is the angle between the director and the propagation direction of light, as shown in Figure 7 [15]. As $\theta(E)$ decreases with the increasing electric field, n_{eff} becomes smaller while n_e and n_o remain constant. Therefore, the central wavelength decreases with an increase in the electric field. The dramatic change of the refractive index leads to a decrease of the central wavelength, although the pitch changes slightly with the unwinding of the helical structure caused by the electric field. After the central wavelength shift of 256 nm by thermal modulation, a central wavelength variation of 76 nm could be obtained at 345 K by electrical modulation.

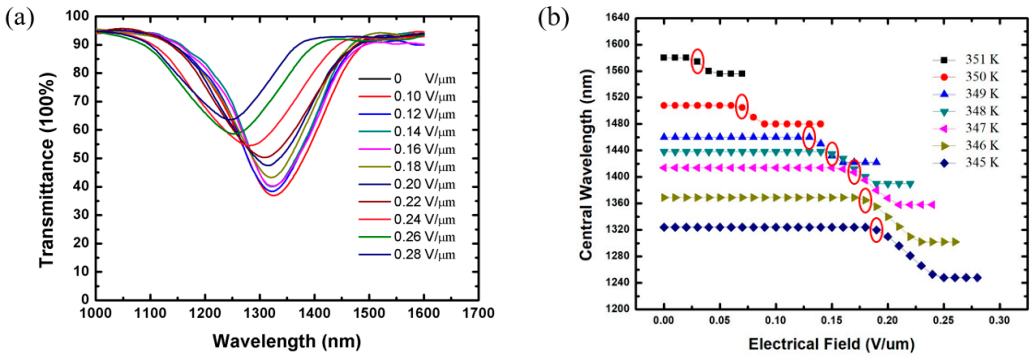

Figure 6. Electric field dependence of (**a**) the transmittance at 345 K and (**b**) the central wavelength at different temperatures in the sphere phase.

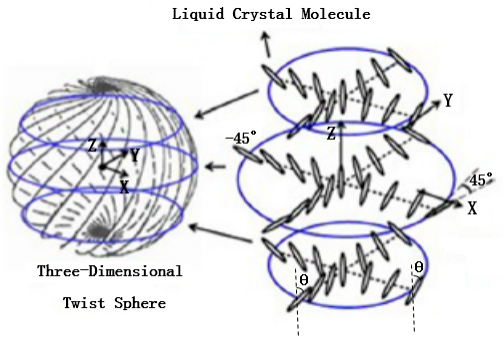

Figure 7. The model of the 3-DTS structure in the sphere phase.

As shown in Figure 6b, both the central wavelength variation and the critical electric field increased with the decrease in temperature. The values of the critical electric fields are marked with red circles in Figure 6b. When the applied electric field is higher than a critical electric field, the LC molecules start tilting. Until the applied electric field increases to a saturated electric field, the LC molecules are reoriented perpendicularly to the substrate plane, and the LC cell transforms into a transparent state with the average refractive index of n_{iso}. In this transparent state, there is no Bragg reflection because there is no periodic structure. With the decrease of temperature, the average refractive index and the viscosity of the LC material increase, resulting in the increase of the central wavelength variation and critical electric field.

4. Conclusions

The transmission properties of SPLC in the NIR region modulated by temperature and electric field were demonstrated. Given the sensitivity of the 3-DTS structures to the external perturbations, the central wavelength could be thermally tuned from 1580 nm to 1324 nm with a temperature-gradient of 42.7 nm/K, and electrically tuned to over 76 nm within a low operating electric field of 0.3 V/μm. Thus, the SPLC filter may achieve a wavelength variation of 256 nm by thermal modulation and 76 nm by electrical modulation. The SPLC filter shows great potential applications in optical communication devices.

Author Contributions: Writing—Original Draft, C.S.; Writing—Review & Editing, J.L.

Funding: This research was funded by National Natural Science Foundation of China, grant number 61727808 and 61775135.

Conflicts of Interest: The authors declare no conflict of interest.

References

1. Fu, Y.; Zhang, J.; Hu, X.; Gong, Q. Electro-optic tunable multi-channel filter in two-dimensional ferroelectric photonic crystals. *J. Opt.* **2010**, *12*, 075202. [CrossRef]
2. Kyoungsik, Y.; Solgaard, O. Tunable optical transversal filters based on a gires-tournois interferometer with mems phase shifters. *IEEE J. Sel. Top. Quantum Electron.* **2004**, *10*, 588–597.
3. Ding, Y.; Pu, M.; Liu, L.; Xu, J.; Peucheret, C.; Zhang, X.; Huang, D.; Ou, H. Bandwidth and wavelength-tunable optical bandpass filter based on silicon microring-mzi structure. *Opt. Express* **2011**, *19*, 6462–6470. [CrossRef] [PubMed]
4. Gan, H.; Zhang, H.; DeRose, C.T.; Norwood, R.A.; Peyghambarian, N.; Fallahi, M.; Luo, J.; Chen, B.; Jen, A.K.Y. Low drive voltage fabry-pérot étalon device tunable filters using poled hybrid sol-gel materials. *Appl. Phys. Lett.* **2006**, *89*, 041127. [CrossRef]
5. Golmohammadi, S.; Moravvej-Farshi, M.K.; Rostami, A.; Zarifkar, A. Narrowband dwdm filters based on fibonacci-class quasi-periodic structures. *Opt. Express* **2007**, *15*, 10520–10532. [CrossRef] [PubMed]
6. Slavik, R.; LaRochelle, S. Large-band periodic filters for dwdm using multiple-superimposed fiber bragg gratings. *IEEE Photonics Technol. Lett.* **2002**, *14*, 1704–1706. [CrossRef]
7. Rumi, M.; White, T.J.; Bunning, T.J. Reflection spectra of distorted cholesteric liquid crystal structures in cells with interdigitated electrodes. *Opt. Express* **2014**, *22*, 16510–16519. [CrossRef]
8. Huang, Y.; Jin, M.; Zhang, S. Polarization-independent bandwidth-variable tunable optical filter based on cholesteric liquid crystals. *Jpn. J. Appl. Phys.* **2014**, *53*, 072601. [CrossRef]
9. Jian-Yu, L.; Johnson, K.M. Analog smectic c * ferroelectric liquid crystal fabry-perot optical tunable filter. *IEEE Photonics Technol. Lett.* **1995**, *7*, 1309–1311. [CrossRef]
10. Wang, C.T.; Jau, H.C.; Lin, T.H. Bistable cholesteric-blue phase liquid crystal using thermal hysteresis. *Opt. Mater.* **2011**, *34*, 248–250. [CrossRef]
11. Lin, J.D.; Huang, S.Y.; Wang, H.S.; Lin, S.H.; Mo, T.S.; Horng, C.T.; Yeh, H.C.; Chen, L.J.; Lin, H.L.; Lee, C.R. Spatially tunable photonic bandgap of wide spectral range and lasing emission based on a blue phase wedge cell. *Opt. Express* **2014**, *22*, 29479–29492. [CrossRef] [PubMed]

12. Huang, Y.; Zhang, S. Widely tunable optical filter with variable bandwidth based on the thermal effect on cholesteric liquid crystals. *Appl. Opt.* **2012**, *51*, 5780–5784. [CrossRef] [PubMed]
13. Hur, S.T.; Lee, B.R.; Gim, M.J.; Park, K.W.; Song, M.H.; Choi, S.W. Liquid-crystalline blue phase laser with widely tunable wavelength. *Adv. Mater.* **2013**, *25*, 3002–3006. [CrossRef] [PubMed]
14. Oton, E.; Netter, E. Wide tunable shift of the reflection band in dual frequency cholesteric liquid crystals. *Opt. Express* **2017**, *25*, 13314–13323. [CrossRef] [PubMed]
15. Zhu, J.L.; Ni, S.B.; Ping Chen, C.; Wu, D.Q.; Song, X.L.; Chen, C.Y.; Lu, J.G.; Su, Y.; Shieh, H.P.D. Chiral-induced self-assembly sphere phase liquid crystal with fast switching time. *Appl. Phys. Lett.* **2014**, *104*, 091116. [CrossRef]
16. Chen, Z.; Hu, D.; Chen, X.; Zeng, D.; Lee, Y.; Chen, X.; Lu, J. Templated sphere phase liquid crystals for tunable random lasing. *Nanomaterials* **2017**, *7*, 392. [CrossRef]
17. Zhu, J.L.; Li, W.H.; Sun, Y.; Lu, J.G.; Song, X.L.; Chen, C.Y.; Zhang, Z.; Su, Y. Random laser emission in a sphere-phase liquid crystal. *Appl. Phys. Lett.* **2015**, *106*, 191903. [CrossRef]
18. Gao, L.; Gao, Y.P.; Du, X.W.; Ye, W.J.; Xu, Q.; Zhu, J.L.; Han, W.M.; Chen, C.Y.; Sun, Y.B. Electro-optical performance of polymer-stabilized sphere phase liquid crystal displays. *Opt. Express* **2017**, *25*, 18009–18016. [CrossRef]
19. Zhou, Y.; Huang, Y.; Ge, Z.; Chen, L.P.; Hong, Q.; Wu, T.X.; Wu, S.T. Enhanced photonic band edge laser emission in a cholesteric liquid crystal resonator. *Phys. Rev. E* **2006**, *74*, 061705. [CrossRef]
20. Mitov, M.; Dessaud, N. Going beyond the reflectance limit of cholesteric liquid crystals. *Nat. Mater.* **2006**, *5*, 361–364. [CrossRef]
21. Tasolamprou, A.C.; Mitov, M.; Zografopoulos, D.C.; Kriezis, E.E. Theoretical and experimental studies of hyperreflective polymer-network cholesteric liquid crystal structures with helicity inversion. *Opt. Commun.* **2009**, *282*, 903–907. [CrossRef]
22. Meiboom, S.; Sethna, J.P.; Anderson, P.W.; Brinkman, W.F. Theory of the blue phase of cholesteric liquid crystals. *Phys. Rev. Lett.* **1981**, *46*, 1216–1219. [CrossRef]
23. Muševič, I.; Žekš, B.; Blinc, R.; Jansen, L.; Seppen, A.; Wyder, P. Temperature dependence of the pitch of the helix in a chiral ferroelectric smectic liquid crystal. *Ferroelectrics* **1984**, *58*, 71–77. [CrossRef]
24. Rout, D.K.; Jain, S.C. Refractive index and microscopic studies of polymer dispersed liquid crystal films containing low concentration of liquid crystals. *Jpn. J. Appl. Phys.* **1991**, *30*, L1412–L1414. [CrossRef]
25. Gharde, R.; Bhave, M.G. The study of refractive indices of liquid crystal mixtures. *Mol. Cryst. Liq. Cryst.* **2015**, *613*, 1–15. [CrossRef]
26. Pajeda, S.; Pajediene, S.; Vaisnoras, R.; Adomenas, P.; Rogante, M. Polarization features of the deformed pdlc film. *Mol. Cryst. Liq. Cryst. Sci. Technol. Sect. A Mol. Cryst. Liq. Cryst.* **2000**, *351*, 43–49. [CrossRef]